DRAFT v.October 15, 2010
Preprint typeset using LaTeX style emulateapj v. 04/20/08

DUST IN THE DIFFUSE EMISSION OF THE GALACTIC PLANE THE *HERSCHEL*/*SPITZER* SED FITTING*

M. Compiègne[1], N. Flagey[2], A. Noriega-Crespo[2], P. G. Martin[1, 3], J.-P. Bernard[4], R. Paladini[2], S. Molinari[5]

DRAFT v.October 15, 2010

ABSTRACT

The first *Herschel* Hi-Gal images of the galactic plane unveil the far-infrared diffuse emission of the interstellar medium with an unprecedented angular resolution and sensitivity. In this paper, we present the first analysis of these data in combination with that of *Spitzer* GLIMPSE & MIPSGAL. We selected a relatively diffuse and low excitation region of the $l \sim 59°$ Hi-Gal Science Demonstration Phase field to perform a pixel by pixel fitting of the 8 to 500 μm SED using the `DustEM` dust emission model. We derived maps of the Very Small Grains (VSG) and Polycyclic Aromatic Hydrocarbons (PAH) abundances from the model. Our analysis allows us to illustrate that the Aromatic Infrared Bands (AIB) intensity does not trace necessarily the PAH abundance but rather the product of "abundance × column density × intensity of the exciting radiation field". We show that the spatial structure of PACS 70 μm map resembles the shorter wavelengths (e. g. IRAC 8 μm) maps, because they trace both the intensity of exciting radiation field and column density. We also show that the modeled VSG contribution to PACS 70 μm (PACS 160 μm) band intensity can be up to 50% (7%). The interpretation of diffuse emission spectra at these wavelengths must take stochastically heated particles into account. Finally, this preliminary study emphasizes the potential of analyzing the full dust SED sampled by *Herschel* and *Spitzer* data, with a physical dust model (`DustEM`) to reach the properties of the dust at simultaneously large and small scales.

Subject headings: methods: data analysis - ISM: dust - infrared: ISM

1. INTRODUCTION

The first *Herschel* (Pilbratt et al. 2010) images of the galactic plane obtained during the Science Demonstration Phase (SDP) reveal with an unprecedented beauty and detail the far-infrared diffuse emission of the interstellar medium (ISM). The Hi-Gal project (Molinari et al. 2010) provides an unbiased photometric survey of the inner Galactic plane emission between 70 and 500 μm where the spectral energy distribution (SED) is dominated by the largest dust grains ($a \sim 0.1\,\mu$m). Combined with the *Spitzer* GLIMPSE (Churchwell et al. 2009) and MIPSGAL (Carey et al. 2009) surveys that cover the dust SED from 3.6 to 24 μm, light mostly emitted by the smallest grains ($a \lesssim 10$ nm), we will for the first time reliably sample the full dust SED of the diffuse emission at all spatial scales down to $\sim 40''$ and over a large fraction of the galactic plane.

At 70 and 160 μm many of the observed structures show a close spatial correlation with some of the classical infrared tracers of small dust particles, like the emission measured at 8 and 24 μm, and therefore, one expects a partially similar origin and/or a similar dependence to ISM physical properties. To properly understand the origin of this emission is the first step of the data analysis.

Dust is heated by stellar ultraviolet(UV)-visible photons and re-radiate the absorbed energy in the infrared. Assuming some dust properties, this dust emission is widely used to trace crucial quantities like cloud masses or star forming activity. However, to derive accurately these quantities requires to take into account the dust properties evolution, how it affects its emission and how it reflects the ISM properties. On the other hand, dust plays a crucial role for the ISM physics and chemistry. Since dust and the rest of ISM are tightly interlock, changes on the dust properties affect those of the gas phase. It is then necessary to characterize the physical processes responsible for the dust evolution to assess their role within the ISM lifecycle and to be able to use dust as a reliable tracer of the ISM. Accessing the full dust SED over a large fraction of the sky allows to follow the behavior of every dust component over a broad range of physical conditions which is an invaluable information for the study of the dust evolution.

In this paper, we present the first analysis of the Hi-Gal data combined with that of GLIMPSE and MIPSGAL to obtain the full dust SED from 8 to 500 μm. In the section 2, we describe the observations and the fitting method that makes use of a physical dust model, `DustEM`[6] (Compiègne et al. 2010). In the section 3, we present and discuss the results and how our analysis method allows us

HERSCHEL IS AN ESA SPACE OBSERVATORY WITH SCIENCE INSTRUMENTS PROVIDED BY EUROPEAN-LED PRINCIPAL INVESTIGATOR CONSORTIA AND WITH IMPORTANT PARTICIPATION FROM NASA. SPITZER SPACE TELESCOPE IS OPERATED BY THE JET PROPULSION LABORATORY, CALIFORNIA INSTITUTE OF TECHNOLOGY UNDER A CONTRACT WITH NASA

Electronic address: compiegne@cita.utoronto.ca
[1] Canadian Institute for Theoretical Astrophysics, University of Toronto, 60 St. George Street, Toronto, ON M5S 3H8, Canada
[2] Spitzer Science Center, California Institute of Technology, 1200 East California Boulevard, MC 220-6, Pasadena, CA 91125, USA
[3] Department of Astronomy & Astrophysics, University of Toronto, 50 St. George Street, Toronto, ON M5S 3H4, Canada
[4] Centre d'Etude Spatiale des Rayonnements, CNRS et Université Paul Sabatier-Toulouse 3, Observatoire Midi-Pyrénées, 9 Av. du Colonel Roche, 31028 Toulouse Cedex 04, France
[5] INAF-Istituto Fisica Spazio Interplanetario, Via Fosso del Cavaliere 100, I-00133 Roma, Italy

[6] To be found at http://www.ias.u-psud.fr/DUSTEM

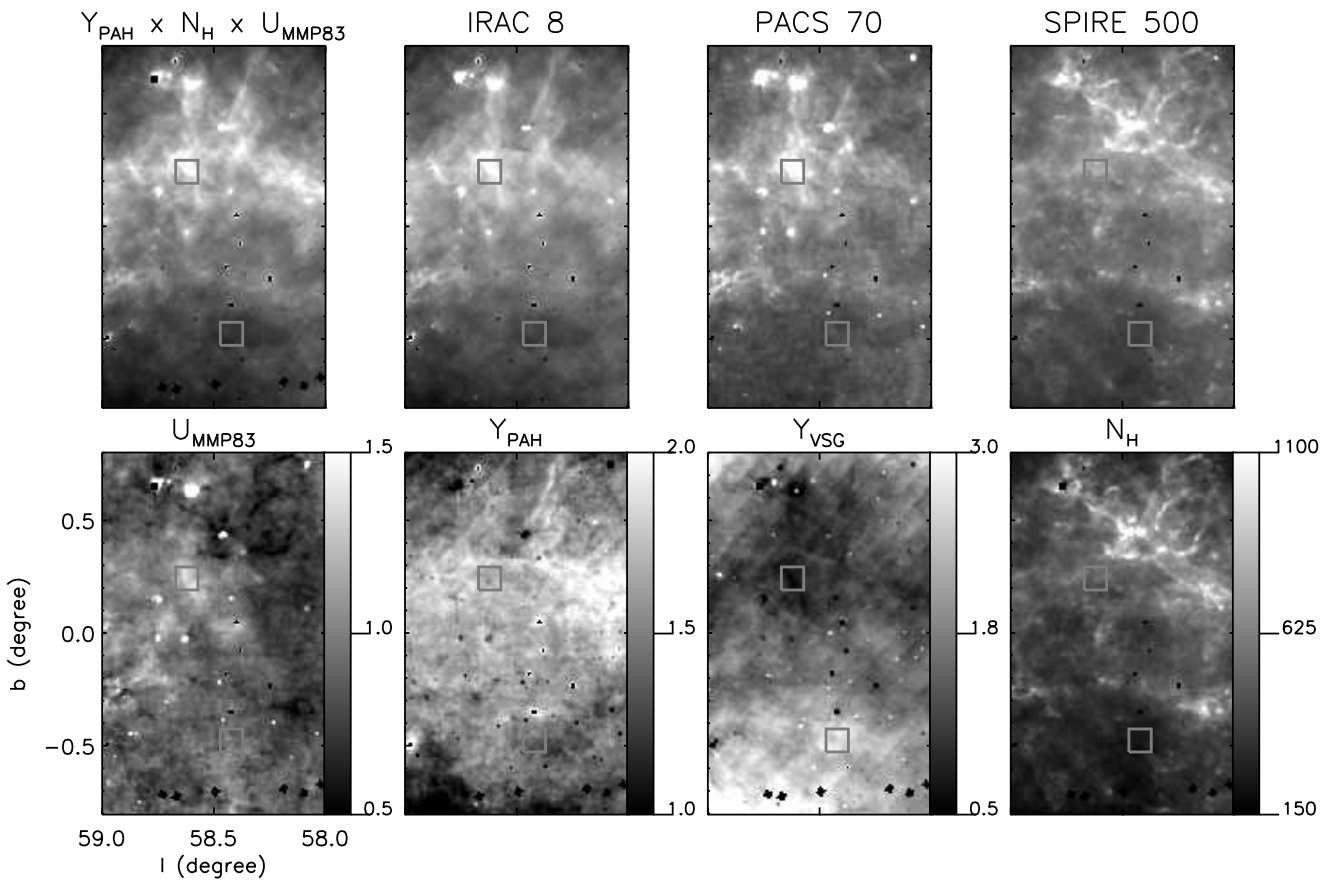

FIG. 1.— IRAC 8 μm, PACS 70 μm and SPIRE 500μm maps. The obtained maps for the fitted parameters are Y_{PAH}, Y_{VSG}, N_H and U_{MMP83}. Also shown is a map of the product $Y_{PAH} \times N_H \times U_{MMP83}$.The two boxes delineate the areas used to obtain the spectra of Fig. 2. Note that the black spots are due to pixel masking (e.g. 8 μm point sources).

to better interpret the behavior of extended emission observed with the *Herschel/Spitzer* photometers. We conclude in the section 4.

2. OBSERVATIONS & ANALYSIS METHOD

Two fields were observed (at $l \sim 30°$ and $l \sim 59°$) during the SDP as part of the Hi-Gal program with PACS 70 and 160 μm and all the SPIRE channels (Molinari et al. 2010). For this study, to satisfy the assumptions made in the model we describe below, we focus on a subfield of the $l \sim 59°$ field that shows no obvious HII regions or young stars cluster and that is relatively diffuse regarding the rest of the $l \sim 59°$ field and the $l \sim 30°$ field. We also avoid the higher latitudes ($|b| \gtrsim 0.8°$) that display weak intensity where *Herschel* data could be less reliable at this early stage of data processing. The maps were obtained with the ROMAGAL pipeline (Traficante et al., 2010, MNRAS, submitted). For PACS 160 μm, SPIRE 250, 350 and 500 μm, we applied the calibration described in Bernard et al. (2010). The gain uncertainty for these data is taken to be 20%. The zero level was corrected by cross-calibration with Planck data with absolute uncertainties of $\pm$ 19.8, 14.6, 7.5 and 3.0 MJy sr^{-1} at 160, 250, 350 and 500 μm, respectively, which represent about half of the gain uncertainty for the faintest pixels of the studied region. We cross-calibrate the PACS 70 μm data with the MIPS 70 μm data from the MIPSGAL survey (Paladini et al., 2010, in prep). We then apply the 15% gain uncertainty of MIPS 70 μm. We also use the IRAC 8 μm data from the GLIMPSE survey and the MIPS 24 μm data from the MIPSGAL survey. The gain uncertainty for these two dataset is taken to be 10%. Point sources are subtracted from the IRAC 8 μm data.

The zodiacal light contribution, important at shorter infrared wavelengths (Kelsall et al. 1998) has been removed from all the *Spitzer* data (on average, 1.1, 16.5 and 4.5 MJy sr^{-1} at 8, 24 and 70 μm, respectively) and then from the PACS 70 μm following its cross-calibration on MIPS 70 μm. We do not perform any subtraction of the zodiacal emission at longer wavelenghts where its contribution is negligible (< 1 MJy sr^{-1}). We bring every map to the lowest resolution of the SPIRE 500 μm one (FWHM $\sim$ 37″). We do this assuming a Gaussian Point Spread Function of appropriate width. We then project all maps into the SPIRE 500 μm grid (pixel field of view $\sim$ 11.5″). Fig. 1 displays the IRAC 8 μm, PACS 70 μm and SPIRE 500 μm maps.

We use the `DustEM` dust model described in Compiègne et al. (2010) to analyse the data. We consolidated the standard four grain populations into three: the Polycyclic Aromatic Hydrocarbons (PAH), Small Amorphous Carbons representing the Very Small Grains (VSG) and we merged Large Amorphous Carbons and Silicates into a single Big Grains (BG) population. Using the MPFIT (Markwardt 2009) IDL minimization routine[7],

[7] To be found at http://purl.com/net/mpfit

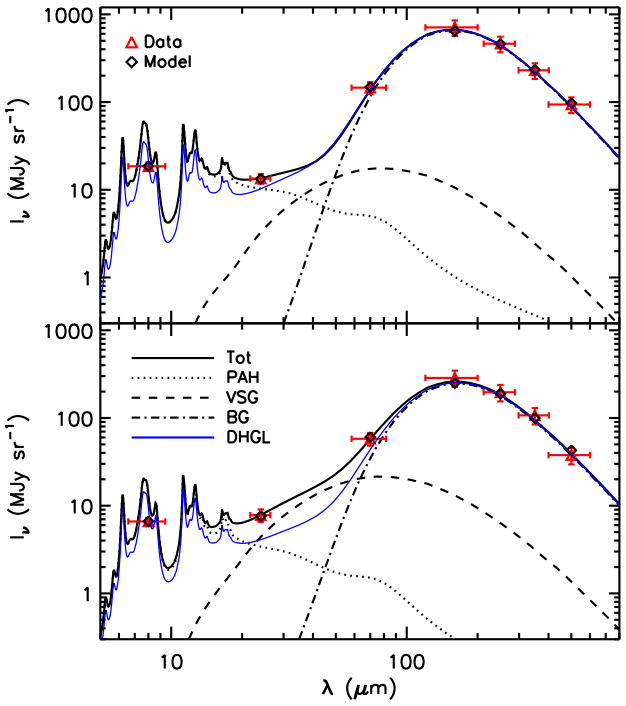

FIG. 2.— Mean spectra over the boxes shown on Fig. 1 and corresponding fitted model. The upper (lower) spectrum correspond to the northern (southern) box. For comparison, the blue lines show the spectra obtain for the fitted N_H and U_{MMP83} but for the reference diffuse high galactic latitude dust properties (DHGL, Y_{PAH} and $Y_{VSG} = 1$).

we choose to adjust the following four parameters to fit the observed SED for each pixel: the (i) PAH and (ii) VSG abundances relative to BG, Y_{PAH} and Y_{VSG}, (iii) the BG opacity, τ_{BG}, and (iv) U_{MMP83} a scaling factor of the "solar neighborhood" Mathis et al. (1983) (hereafter MMP83) exciting radiation field. Self-extinction along the line of sight can be significant at 8 μm and is accounted for assuming $I_\lambda = I_{0,\lambda} \frac{1-e^{-\tau_\lambda}}{\tau_\lambda}$ where $I_{0,\lambda}$ is the integrated emissivity and τ_λ the total dust opacity that is computed from the dust model using Y_{PAH}, Y_{VSG} and τ_{BG}. Since in this first analysis we do not perform any separation of the components along the line of sight, the derived parameters result from the spatial mixing of different physical conditions. Fortunately, at $l \sim 59°$, we expect only contributions from the Vulpecula star formation region (d$\sim$2 kpc) and the Perseus arm (d$\sim$8.5 kpc).

We focus on the smallest particles behavior (PAH and VSG) and hence, we do not assume any variation of the BG properties (i.e. $\tau_{BG}/N_H =$ constant). In that case and to ease the following discussion, we can convert τ_{BG} into the hydrogen column density, N_H, and assume the relative abundances of PAH and VSG, Y_{PAH} and Y_{VSG} to be their abundance relative to hydrogen. Indeed, emissivity and/or abundance of the BG is known to evolve (e.g. Stepnik et al. 2003; Désert et al. 2008) and can be studied using the *Herschel* data (see Paradis et al. 2010) but to take such variations into account is beyond the scope of this paper.

Fig. 2 illustrates the obtained fitted spectra for two observed SEDs. The photometric points computed from a modeled spectrum take into account the color corrections. Schematically, the 160, 250, 350 and 500 μm photometric points give constraints on U_{MMP83} and τ_{BG} (N_H) through the BG emission. The shape of the BG SED depends on U_{MMP83} as this grain population is at thermal equilibrium, in contrast with the stochastically heated grains (PAH and VSG) whose SED shape is invariant regarding the radiation field intensity (see Draine & Li 2007; Compiègne et al. 2010). Hence, given U_{MMP83} the absolute level of the BG SED constrains N_H. Finally, the 8 and 24 μm constrain the abundances of the two stochastically heated population since the intensity of their emission scales as $Y \times N_H \times U_{MMP83}$.

3. RESULTS & DISCUSSION

Fig. 1 shows maps of the Y_{PAH}, Y_{VSG}, N_H and U_{MMP83} parameters and a map of the product $Y_{PAH} \times N_H \times U_{MMP83}$. $\chi^2_{reduced} \lesssim 2$ for all pixels over these maps. N_H is given in unit of $10^{20}\,H\,cm^{-2}$ and U_{MMP83} is dimensionless. Y_{PAH} and Y_{VSG} are given relative to the value for the diffuse high galactic latitude medium (DHGL, $|b| \gtrsim 15°$), $M_{PAH}/M_H = 7.8\,10^{-4}$ and $M_{VSG}/M_H = 1.65\,10^{-4}$ (see Compiègne et al. 2010). Notice that $M_{BG}/M_H = 9.25\,10^{-3}$. The uncertainties on these parameters are given as computed in MPFIT from the covariance matrix.

The column density lies between $\sim$1.5 $10^{22}\,H\,cm^{-2}$ for the most diffuse part and $\sim$1.1 $10^{23}\,H\,cm^{-2}$ toward the dense filamentary structures, with a relative uncertainty of $\sim$18%. The U_{MMP83} ranges between $\sim$0.5 and $\sim$1.5 with a relative uncertainty of $\sim$22%, which is consistent with the absence of young stellar cluster over our field. In agreement with the fact that the radiation field is shielded, we see that U_{MMP83} decreases toward the highest column density regions. These U_{MMP83} and N_H values are in agreement with previous estimates (see Bernard et al. 2010). Y_{PAH} goes from $\sim$1.0 to $\sim$2.0 with a relative uncertainty of $\sim$16%. The obtained Y_{VSG} spans a wider range than Y_{PAH}, going from $\sim$0.5 to $\sim$3.0 but with a relative uncertainty going from $\sim$40% for the highest values to $\sim$60% for the smallest values. The variations of these parameters over the map are therefore significant.

Fig. 2 shows the averaged SED over the two boxes seen on Fig. 1 and illustrate the wide Y_{VSG} variations. For the top (bottom) panel spectrum we have $N_H = 5.1\pm0.9\,10^{22}\,H\,cm^{-2}$ ($2.5\pm0.5\,10^{22}\,H\,cm^{-2}$), $U_{MMP83} = 1.2\pm0.2$ (0.9 ± 0.2), $Y_{PAH} = 1.7\pm0.2$ (1.4 ± 0.2) and $Y_{VSG} = 0.8\pm0.5$ (2.7 ± 1.0).

Y_{PAH}/Y_{VSG} seems to vary at large spatial scales (decreases from $b \sim 0.2°$ to $b \sim -0.7°$) and also at the edge of some dense filaments (near the "chimney" region around coordinate 58.4, +0.55). Both Y_{PAH} and Y_{VSG} decrease towards some of the densest filamentary structures but it appears not to be systematic and could be biased by the too simplistic assumption made on the self-absorption. A decrease of the smallest dust abundance towards dense regions regarding the biggest grains was reported by previous work and was interpreted as the coagulation of these smallest particles together with the bigger ones (e.g. Stepnik et al. 2003; Flagey et al. 2009). Previous studies also reported a lack of correlation or even an anti-correlation between the aromatic infrared bands and the mid-IR continuum emission (interpreted as the evolution of small dust properties) at the illumi-

nated ridge of molecular clouds (e.g. Abergel et al. 2002; Berné et al. 2007; Compiègne et al. 2008), toward high galactic cirrus at the interface between atomic and molecular material (Miville-Deschênes et al. 2002) or at galactic scale in the Large Magellanic Cloud (Paradis et al. 2009).

The spatial structure of SPIRE 500 μm intensity, that is dominated by the BG contribution, is well correlated with N_H. Indeed, U_{MMP83} and subsequently the BG temperature is quite stable in our field so that the intensity variations at these wavelengths (Rayleigh tail of the blackbody like emission) are dominated by the column density variations (assuming no BG emissivity variations). Comparing the 8 μm and Y_{PAH} maps, it is striking that the AIB intensity does not directly trace the PAH abundance. PAH are stochastically heated and the observed AIB intensity (i.e. IRAC 8 μm) then scales linearly with the product $Y_{PAH} \times N_H \times U_{MMP83}$ as seen on Fig. 1. The only difference is related to the extinction along the line of sight that can be seen in the IRAC 8 μm (as dark filamentary structures correlated with the N_H map) and not in the $Y_{PAH} \times N_H \times U_{MMP83}$ map. The PACS 70 μm image shows a close spatial correlation with the classical infrared tracers of small dust particles, like the emission measured at 8 μm (see Fig. 1). The emission at 70 μm is not due to a single dust component. As seen on Fig 2, in the framework of our model both the VSG that are stochastically heated and the BG that are at thermal equilibrium contribute to the emission at this wavelength. For $U_{MMP83} \lesssim 100$, the BG emission at 70 μm fall in the Wien part of the blackbody like emission that makes it more sensitive to U_{MMP83} than at 500 μm. Therefore, the two emission components (from VSG and BG) at 70 μm are sensitive to both N_H and U_{MMP83} explaining the better correlation of this map with the 8 μm map (also sensitive to both N_H and U_{MMP83}) than with the 500 μm map (more sensitive to N_H).

The model allows us to compute the relative contribution of the three dust populations in the different photometric bands. The VSG contribution to PACS 70 μm increases if the VSG abundance relative to BG increases and/or if U_{MMP83} decreases (shifting the BG emission toward longer wavelengths). In the studied field, the VSG contribution to the PACS 70 μm intensity goes from $\sim$ 10% up to $\sim$ 50% with a median value of $\sim$ 27%. The maximum contribution of VSG to PACS 100 μm and PACS 160 μm is $\sim$ 17% and $\sim$ 7% (the median is 9% and 3%), respectively. For the top (bottom) panel spectrum of Fig. 2, the contribution is 12, 4, 2% (35, 13, 5%) for PACS 70, 100 and 160 μm, respectively. This result strongly suggests that the proper analysis of *Herschel* spectrum of diffuse emission including 70 μm may require to account for stochastically heated grains.

4. SUMMARY & CONCLUSION

We have presented the first analysis of the diffuse emission of the galactic plane as observed by *Herschel* combining the Hi-Gal data with the GLIMPSE/MIPSGAL *Spitzer* data. Toward a subfield of the l$\sim$ 59° Hi-Gal SDP field, we performed a pixel by pixel fitting of the full dust SED between 8 and 500 μm using a physical dust emission model, `DustEM` (Compiègne et al. 2010).

Assuming that the BG properties remain constant, the unique wavelength coverage provided by the *Spitzer* and *Herschel* photometric observations allows us to derive the following parameters for our dust model : the PAH and VSG abundances, Y_{PAH} and Y_{VSG}, the column density, N_H, and the intensity of the exciting radiation field, U_{MMP83}. To our knowledge, this is the first time PAH and VSG abundance maps are derived using such a pixel by pixel SED fitting at resolution $< 1'$ and over such an extended field. These abundances, as well as N_H and U_{MMP83}, vary significantly over the field. As already reported by previous studies, Y_{PAH} and Y_{VSG} appears not to be positively correlated.

Although it was already theoretically known, our analysis method provide a firm demonstration that IRAC 8 μm does not trace the PAH abundance but the product $Y_{PAH} \times N_H \times U_{MMP83}$. We also showed that at 70 μm, the modeled emission is due to both the BG and the VSG. At these wavelengths the BG emission is sensitive to both the intensity of the exciting radiation field and the column density likewise the VSG, explaining the similar spatial structure seen in PACS 70μm maps regarding shorter wavelengths. Using our model, we derived the VSG contribution to the PACS channels that can be up to $\sim$ 50%, $\sim$ 17% and $\sim$ 7% at 70, 100 and 160 μm, respectively. We conclude that the interpretation of *Herschel* spectrum of the diffuse emission down to 70 μm may require to take into account the stochastically heated population (VSG).

Finally, our analysis allows for a better understanding of the first *Herschel* images of the galactic plan diffuse emission by disentangling between the different dust population contributions and also revealing the great potential of the *Herschel*/*Spitzer* synergy combined with a physical dust model for the study of dust evolution (see also Abergel et al. 2010).

REFERENCES

Abergel, A., et al. 2002, A&A, 389, 239
—. 2010, A&A, 518, L96+
Bernard, J., et al. 2010, A&A, 518, L88+
Berné, O., et al. 2007, A&A, 469, 575
Carey, S. J., et al. 2009, PASP, 121, 76
Churchwell, E., et al. 2009, PASP, 121, 213
Compiègne, M., Abergel, A., Verstraete, L., & Habart, E. 2008, A&A, 491, 797
Compiègne, M., et al. 2010, A&A, in press
Désert, F.-X., et al. 2008, A&A, 481, 411
Draine, B. T., & Li, A. 2007, ApJ, 657, 810
Flagey, N., et al. 2009, ApJ, 701, 1450
Kelsall, T., et al. 1998, ApJ, 508, 44
Markwardt, C. B. 2009, in Astronomical Society of the Pacific Conference Series, Vol. 411, Astronomical Society of the Pacific Conference Series, ed. D. A. Bohlender, D. Durand, & P. Dowler, 251–+
Mathis, J. S., Mezger, P. G., & Panagia, N. 1983, A&A, 128, 212
Miville-Deschênes, M.-A., Boulanger, F., Joncas, G., & Falgarone, E. 2002, A&A, 381, 209
Molinari, S., et al. 2010, A&A, 518, L100+
Molinari, S., et al. 2010, PASP, 122, 314
Paradis, D., et al. 2009, AJ, 138, 196
—. 2010, A&A, 520, L8+
Pilbratt, G. L., et al. 2010, A&A, 518, L1+
Stepnik, B., et al. 2003, A&A, 398, 551